Journal of Nuclear Materials 392 (2009) 364–370

Contents lists available at ScienceDirect

Journal of Nuclear Materials

journal homepage: www.elsevier.com/locate/jnucmat

The Influence of lithium environment on tensile behavior and microstructure of V–4Cr–4Ti

Meimei Li [a,c,*], D.T. Hoelzer [a], M.L. Grossbeck [b]

[a] Materials Science and Technology Division, Oak Ridge National Laboratory, Oak Ridge, TN 37831, USA
[b] Nuclear Engineering Department, University of Tennessee, Knoxville, TN 37996, USA
[c] Nuclear Engineering Division, Argonne National Laboratory, 9700 S. Cass Avenue, Argonne, IL 60439-4838, USA

A B S T R A C T

Thermal tests exposed V–4Cr–4Ti in static liquid lithium at 700 and 800 °C for 250, 500, and 1000 h. Post-exposure examination included chemical analysis of interstitial impurities in V–4Cr–4Ti to monitor impurity transfer, and tensile tests at room temperature and 500 °C. Microstructures were characterized by room-temperature electrical resistivity measurements and transmission electron microscopy. Oxygen was not depleted from V–4Cr–4Ti when nitrogen pickup occurred during lithium exposures. In spite of a significant increase in interstitial impurity concentration, the matrix interstitial solute content was reduced due to precipitation. Plate-shaped precipitates in the matrix and globular precipitates at grain boundaries were formed during lithium exposures at 700 °C, while only globular precipitates were observed at grain boundaries at 800 °C. Increases in strength, decreases in ductility, and reduced dynamic strain aging resulted. Ductility remained high after 1000 h exposures at both 700 and 800 °C.

1. Introduction

Liquid metal is an important heat transfer medium for advanced reactor concepts, including fusion reactors, the GenIV sodium or lead/lead–bismuth-cooled reactors, and the GNEP advanced burner reactors. An understanding of the effects of liquid metal environment on mechanical properties and microstructural evolution is important in identifying material degradation mechanisms, in alloy selection, and in the design of reactor components.

V–4Cr–4Ti is a leading candidate for structural applications in advanced fusion reactors for a lithium–vanadium blanket concept. The application of vanadium alloys in fusion systems depends greatly on their compatibility with liquid lithium. One of the major compatibility issues is the mass transfer of interstitial elements O, C, and N in a vanadium–lithium system [1–3]. When exposed above 500 °C, vanadium tends to lose oxygen to lithium and absorb nitrogen and carbon from the lithium [4]. These changes in interstitial chemistry of vanadium alloys can strongly affect their microstructural stability, mechanical properties, and irradiation behavior [3,5–13]. Continued removal of oxygen from vanadium alloys can lead to loss of high temperature strength, and pickup of nitrogen and carbon from the lithium can cause significant ductility loss of the alloys [11,12]. The distribution of interstitial elements in the alloy matrix can be affected by lithium exposure as well. Free interstitial solutes in vanadium alloys can be removed from the matrix by the precipitation of titanium solute with interstitial elements, resulting in changes in irradiation-induced precipitation, swelling, and mechanical properties [13–17]. Both the formation and the morphology of titanium precipitates depend on annealing temperatures. Titanium is mobile in V–4Cr–4Ti above 600 °C under thermal annealing and above 300 °C under neutron irradiation [9]. Plate-shaped Ti(CON) precipitates usually form below 1000 °C, and globular Ti(CON) precipitates appear above 1000 °C [16–18]. Precipitation behavior of V–4Cr–4Ti is also affected by the level of interstitial impurities in the alloy. Enhanced precipitation was observed in nitrogen-doped V–4Cr–4Ti [14,15,19]. The susceptibility of vanadium alloys to interstitial contamination is more serious when long exposure times are involved.

The interaction of interstitial solutes with Ti atoms in V–4Cr–4Ti has been studied by examining the dynamic strain aging behavior. V–4Cr–4Ti, like other bcc metals and solid solution alloys, exhibits serrated flow when tensile-tested over the temperature range 300–750 °C, and the serration is most pronounced at 500–600 °C at a strain rate of 10^{-3} s^{-1} [20]. This so-called dynamic strain aging effect is associated with the interaction of interstitial solutes with moving dislocations, and it provides the basis for understanding the distribution of interstitial impurities and the

* Corresponding author. Present address: Nuclear Engineering Division, Argonne National Laboratory, 9700 S. Cass Avenue, Argonne, IL 60439-4838, USA. Tel.: +1 630 252 5111; fax: +1 630 252 3604.
E-mail address: mli@anl.gov (M. Li).

0022-3115/$ - see front matter © 2009 Elsevier B.V. All rights reserved.
doi:10.1016/j.jnucmat.2009.03.026

precipitation reaction. The precipitation behavior of V–4Cr–4Ti in lithium environments and its effects on the mechanical properties has not been well studied.

This paper presents experimental results on the influence of lithium exposure on composition, microstructure, and mechanical behavior of V–4Cr–4Ti that was exposed to liquid lithium at 700 and 800 °C for up to 1000 h. Tensile tests were carried out on lithium-exposed specimens at room temperature to measure tensile property changes with increasing exposure time. Specimens were also tested at 500 °C at a strain rate of 1×10^{-3} s^{-1} to examine the dynamic strain aging behavior. As-exposed microstructure was examined by transmission electron microscopy (TEM) to understand the precipitation process. Room-temperature electrical resistivity measurements on lithium-exposed specimens provided further evidence of the distribution of interstitial solutes.

2. Experimental procedure

The material examined was the US Heat 832665 of V–4 wt%Cr–4 wt%Ti. Type SS-J3 sheet tensile specimens were machined from a 3.81 mm thick, 40% cold-rolled R-plate. The SS-J3 specimens had a nominal gauge width of 1.19 mm, gauge length of 5.00 mm and a thickness of 0.75 mm. Following machining the specimens were annealed at 1000 °C for 2 h in high vacuum (1×10^{-5} Pa). The content of interstitial impurities in annealed SS-J3 tensile specimens prior to lithium exposure was 387 wppm (weight parts per million) O, 94 wppm N, and 128 wppm C. Coupon specimens (nominal dimensions of $25 \times 6 \times 3$ mm) were also machined from the same plate and included for each lithium exposure. The initial content of interstitial impurities in coupon specimens prior to lithium exposure was 322 wppm O, 99 wppm N, and 122 wppm C.

Tensile and coupon specimens were exposed to static liquid lithium at 700 and 800 °C for up to 1000 h. Pressurized creep tubes were also included in the lithium exposure tests, and the creep data are reported in [6]. Thermal exposure tests were carried out in static liquid lithium in a test apparatus located in a glove box protected by high purity argon. Details of the test setup are described elsewhere [21,22]. Pure lithium (>99.9%) was supplied by Sigma–Aldrich with a nitrogen content of 161 ppm determined by a modified Kjeldahl procedure. To minimize contamination of lithium metal by nitrogen and carbon, the commercial lithium was either purified by hot-trapping with Zr getters prior to exposure tests, or by loading either Zr or Ti getters in lithium exposure tests. A batch of lithium was used for no more than two exposure tests and then replaced with a new batch. After exposures, all specimens were removed from lithium and cleaned by liquid anhydrous ammonia. Specimens requiring further exposure were reloaded into liquid lithium. This process was repeated at exposure intervals of 255, 499, and 1019 h at 700 °C and at intervals of 260, 515, and 1015 h at 800 °C. For simplicity and clarity, nominal exposure times, i.e. 250, 500, and 1000 h are used in the following sections.

The coupon specimens were used to monitor changes in interstitial impurity content after each exposure condition. Analyses for C, N, and O in unexposed coupon specimens and in coupon specimens after each exposure test were performed by LECO Technical Analysis Lab, and their interstitial chemistry data were reported in this paper. While the coupon specimens were thicker than the SS-J3 tensile specimens used for mechanical properties tests and microstructural analysis, and would have somewhat different rates of mass transfer, changes in composition for the two specimen sizes would follow the same trends for identical exposures. The correlation of interstitial chemistry changes in coupon specimens with tensile and TEM data was to provide a qualitative view of how tensile properties and precipitation behavior were affected by interstitial transfer.

Electrical resistivity was measured at room temperature on the SS-J3 tensile specimens before and after each lithium exposure, using a four-point probe technique. Tensile tests were performed at 20 °C in air and at 500 °C in vacuum (1×10^{-4} Pa) at a strain rate of 1×10^{-3} s^{-1}. The data acquisition rate was 20 points/s. After tensile testing, TEM disks were punched from the grip section and mechanically thinned to 200–250 μm by removing material from both sides. The TEM foils were prepared by electropolishing with a sulfuric acid and methanol electrolyte at −10 °C. The microstructure was examined in a FEI Tecnai 20 electron microscope at 200 kV.

3. Results

3.1. Transfer of interstitial impurities

Fig. 1 shows the changes in the concentration of interstitial elements O, C, and N in V−4Cr–4Ti exposed to lithium with increasing exposure times at 700 and 800 °C. During lithium exposure at 700 °C, a slight increase in nitrogen and carbon and a decrease in oxygen occurred during the first 250 h exposure. Significant pickup of nitrogen was observed during further exposure up to 1000 h at an average pickup rate of 0.32–0.36 wppm N/h. Slight pickup of carbon was also observed during exposure from 250 to 500 h. Surprisingly, the concentration of oxygen in V–4Cr–4Ti was nearly unchanged even after exposure for 1000 h. The total contents of interstitial impurities increased from

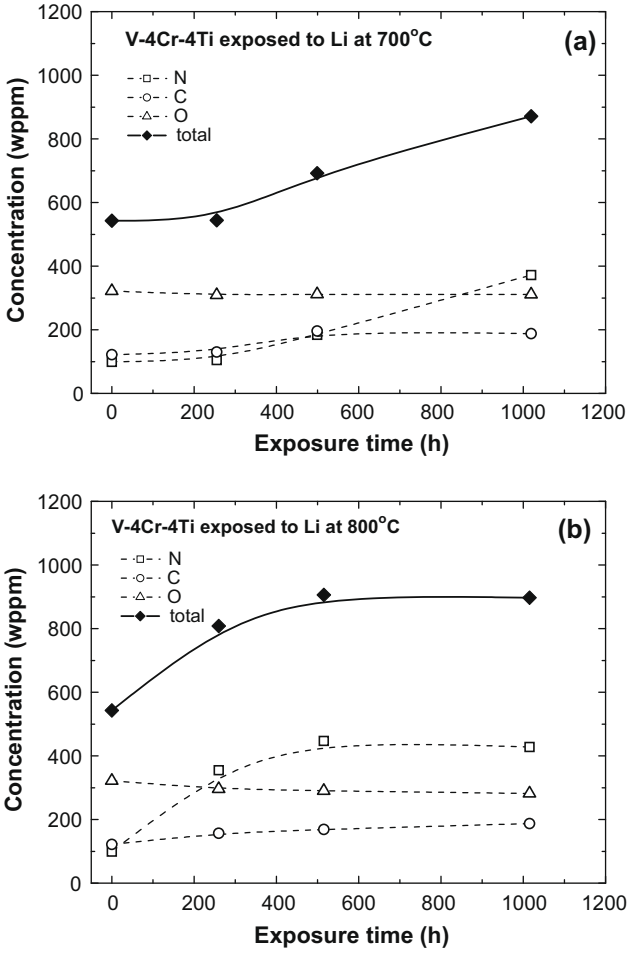

Fig. 1. Interstitial impurity concentration as a function of exposure time in V–4Cr–4Ti exposed to lithium at (a) 700 °C and (b) 800 °C.

the initial value of 543 wppm to 871 wppm after exposure for 1000 h. Pickup of nitrogen dominates overall interstitial concentration increase.

Significant pickup of nitrogen occurred during lithium exposure at 800 °C as well. The rate of nitrogen pickup was 0.98 wppm N/h during the first 250 h exposure and was reduced to 0.36 wppm N/h during exposure from 250 to 500 h. The concentration of nitrogen was slightly decreased during exposure from 500 to 1000 h. Slight pickup of carbon was observed. Only a small decrease in oxygen content was found, with 40 wppm O decrease after exposure for 1000 h. The overall content of interstitial impurities was 897 wppm after 1000 h exposure at 800 °C. Again, the increase of the total interstitial concentration is dominated by the nitrogen increase.

3.2. Tensile properties after lithium thermal exposure

Tensile specimens exposed to lithium at 700 °C for 250, 500, and 1000 h were tested at room temperature. The stress–strain curves are shown in Fig. 2(a), and the tensile properties, i.e. yield stress (YS) (the lower yield stress or 0.2% offset yield stress if there is no yield point), ultimate tensile strength (UTS), uniform elongation (UE), and total elongation (TE) are plotted in terms of exposure time in Fig. 2(b). The unexposed specimen exhibited pronounced yield-point behavior, i.e. upper and lower yield points and Lüders strain after the elastic regime. Exposure to lithium reduces the yield point effect. The magnitude of the yield drop and the Lüders strain decreased with increasing exposure time. The yield points and Lüders strain disappeared after 1000 h exposure. The yield stress slightly increased after 250 h exposure, increased significantly after 500 h exposure, and then decreased at 1000 h, while the ultimate tensile stress continuously increased with increasing exposure time for a total increase of 60 MPa at 1000 h. The strain hardening effect in the 1000 h-exposed specimen was notably higher than that in all other specimens. Both uniform elongation and total elongation decreased with increasing time. The alloy still had a total elongation of 24% after 1000 h exposure.

The tensile specimens exposed to liquid lithium at 800 °C for 250, 500, and 1000 h were also tested at room temperature, and the stress–strain curves are shown in Fig. 3(a). The tensile properties are plotted in Fig. 3(b) as a function of exposure time. The yield-point in the stress–strain curves diminished with increasing exposure time. The magnitude of the yield drop in the 250 h-exposed specimen is considerably smaller than in the unexposed specimen. Further exposure to 500 and 1000 h completely removed the Lüders strain and yield points. The yield stress decreased with increasing exposure time with a 48 MPa drop after 1000 h exposure. The ultimate tensile stress increased rapidly with time with a total increase of 111 MPa for 1000 h. Strain hardening became more pronounced as exposure time increased. Both the uniform elongation and the total elongation decreased with

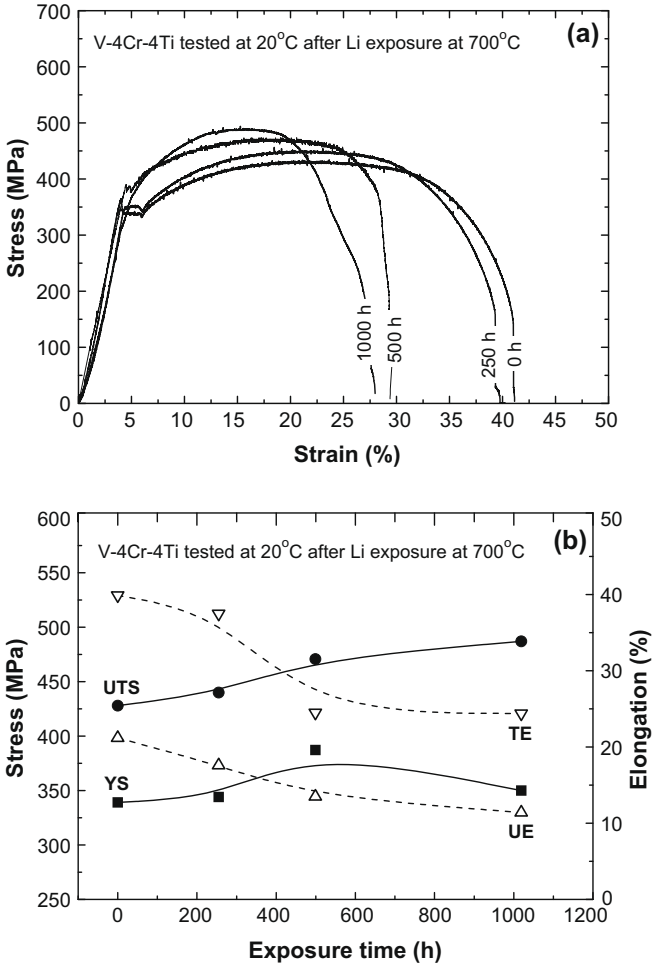

Fig. 2. (a) Stress–strain curves and (b) tensile properties (YS = yield stress, UTS = ultimate tensile strength, UE = uniform elongation, TE = total elongation) of V–4Cr–4Ti exposed to lithium at 700 °C and tested at room temperature.

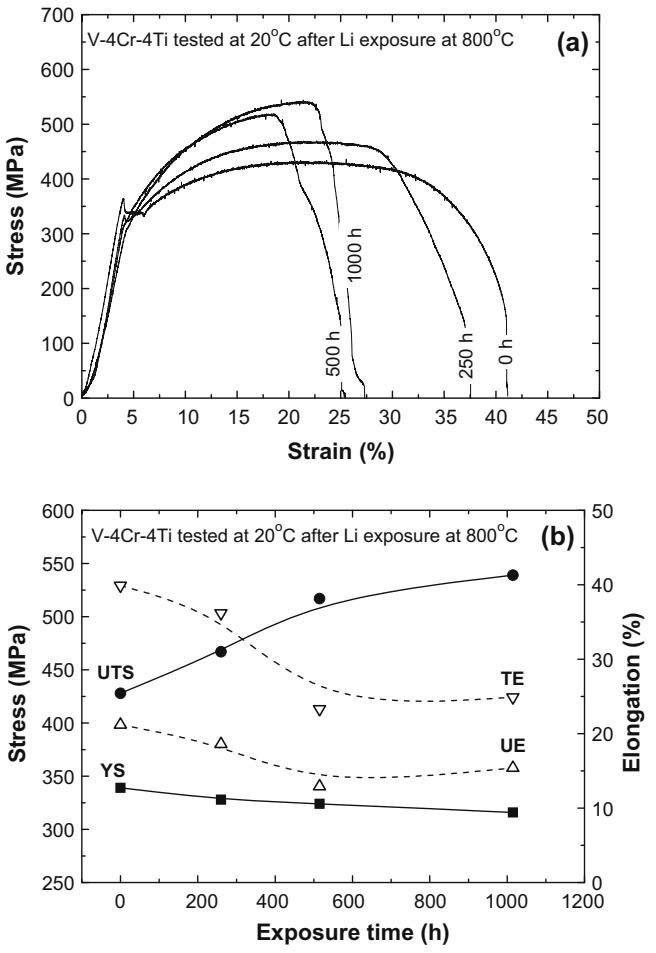

Fig. 3. (a) Stress–strain curves and (b) tensile properties of V–4Cr–4Ti exposed to lithium at 800 °C and tested at room temperature.

exposure time, and yet the alloy still retained 25% ductility after 1000 h exposure.

3.3. Dynamic strain aging at 500 °C after lithium thermal exposure

A set of tensile specimens exposed to lithium at 700 and 800 °C were tested at 500 °C and a strain rate of 1×10^{-3} s^{-1} to examine the dynamic strain aging (DSA) effect in V–4Cr–4Ti. Previous studies showed that all three interstitial solutes C, O, and N contribute to the DSA behavior of vanadium alloys above 400 °C, which is characterized by serrated stress–strain curves [20,23]. The serrations in the flow stress were found to be most evident at 500 °C at a low strain rate (e.g. 10^{-3} s^{-1}) in V–4Cr–4Ti [20]. Fig. 4(a) shows the stress–strain curves of the unexposed specimen and specimens exposed to lithium at 700 °C for 250 and 500 h and tested at 500 °C, and Fig. 4(b) is an exploded view of the tensile curves in the strain range of 10–15% to compare serrations in the flow stress. Pronounced serrations were observed in the flow curves of the unexposed specimen and the 250 h-exposed specimen. Thermal exposure in lithium for 250 h had minimal effects on both the flow behavior and the serrations of the alloy. Note that the interstitial contents were nearly unchanged during the first 250 h exposure. Further exposure to 500 h resulted in the suppression of serrations in the flow curve along with a significant increase in strength and decrease in ductility.

The stress–strain curves of the unexposed specimen and specimens exposed to lithium at 800 °C for 250, 500, and 1000 h and tested at 500 °C are shown in Fig. 5(a), and an exploded view of the tensile curves in the strain range of 10–15% is shown in Fig. 5(b). Serrations in the flow stress decreased and disappeared with increasing exposure time. The amplitude of serrations dropped from 18 MPa in the unexposed specimen to less than 10 MPa in the 250 h-exposed specimen. The strength of the alloy increased and the ductility decreased with exposure time, except that the 1000 h-exposed specimen showed a lower ultimate tensile stress and lower ductility than those of the 500 h-exposed specimen.

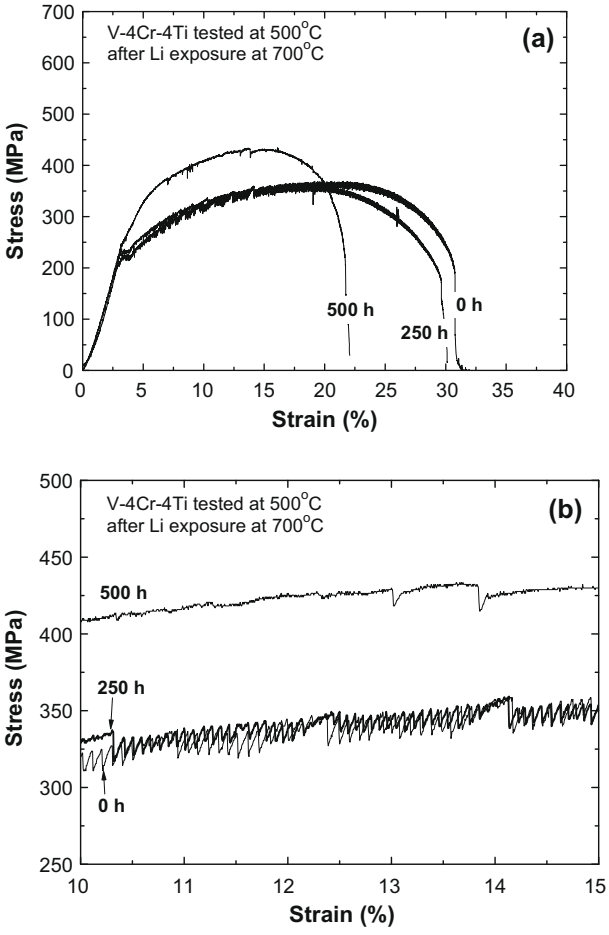

Fig. 4. Stress–strain curves of V–4Cr–4Ti exposed to lithium at 700 °C and tested at 500 °C (a) overview of flow curves, (b) exploded view of flow curves in the strain range from 10% to 15% illustrating serrations and discontinuous yielding.

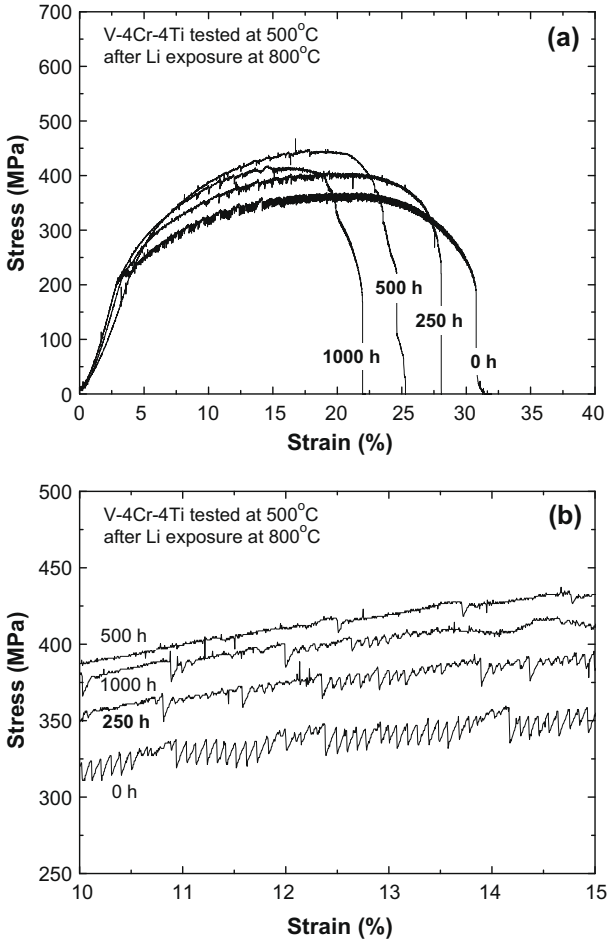

Fig. 5. Stress–strain curves of V–4Cr–4Ti exposed to lithium at 800 °C and tested at 500 °C (a) overview of flow curves, (b) exploded view of flow curves in the strain range from 10% to 15% illustrating serrations and discontinuous yielding.

3.4. Precipitation during lithium thermal exposure

Representative TEM micrographs showing the microstructure of V–4Cr–4Ti following exposure in lithium at 700 °C for 250 h and 1000 h are shown in Fig. 6. After the 250 h exposure, the microstructure consisted of a low number density of non-uniformly distributed plate-shaped precipitates in the matrix (Fig. 6(a)) and fine globular precipitates decorating grain boundaries (Fig. 6(b)). The plate precipitates were ~200–300 nm in diameter and <10 nm thick and the globular precipitates were ~50 nm in size. As exposure time increased, the number density of plate precipitates increased and their distribution in the matrix became more uniform. The sizes of both matrix precipitates and grain boundary precipitates slightly increased, as seen in Figs. 6(c) and (d) for the 1000 h-exposed specimen. The plate precipitates were found to have a $\{100\}_{bcc}$ habit plane with the matrix and diffuse streaks parallel to $\langle 100\rangle_{bcc}$ with intensity maxima at $\frac{3}{4}\langle 200\rangle$ in selected

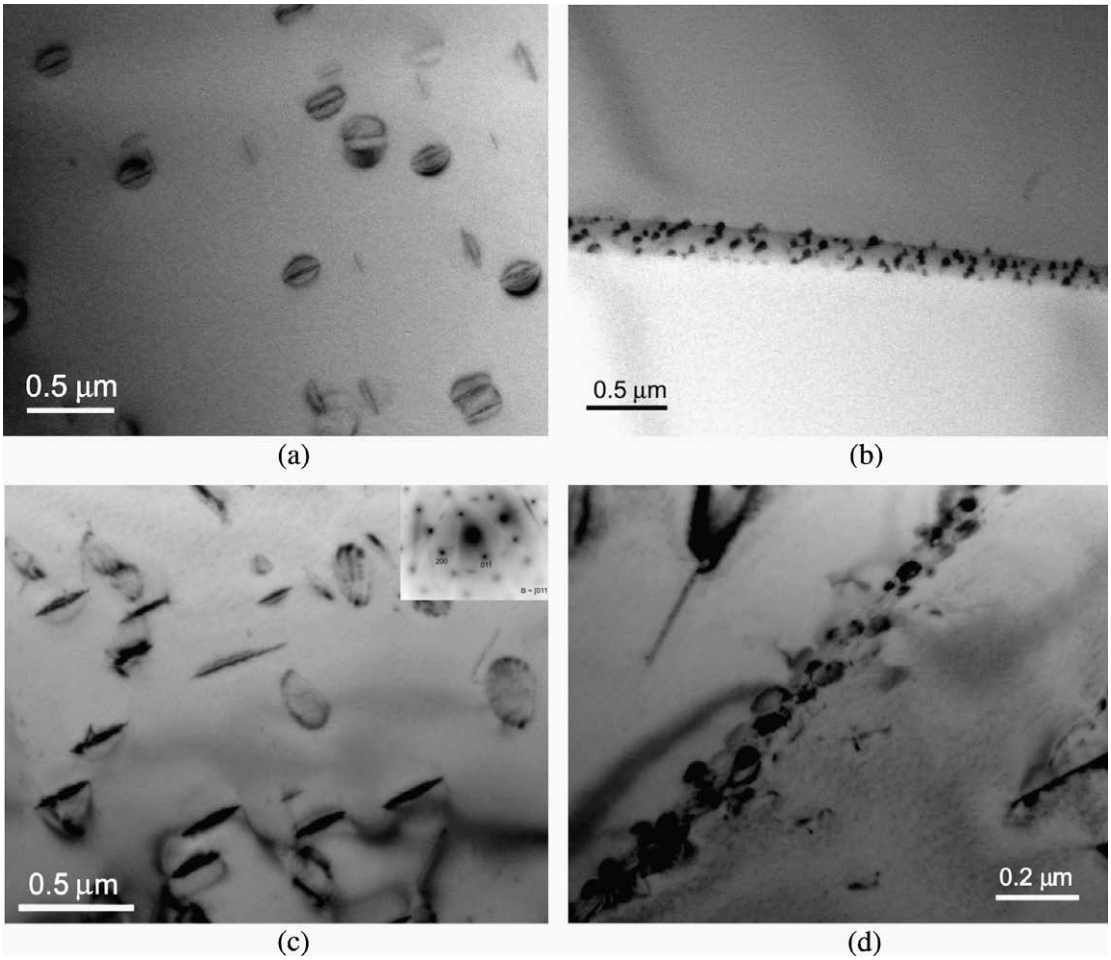

Fig. 6. Representative TEM micrographs showing (a) plate-shaped precipitates in the grain interior and (b) spherical precipitates at grain boundaries in the specimen exposed to lithium at 700 °C/250 h, and (c) plate-shaped precipitates in the grain interior (d) spherical precipitates at grain boundaries in the specimen exposed to lithium at 700 °C/1000 h.

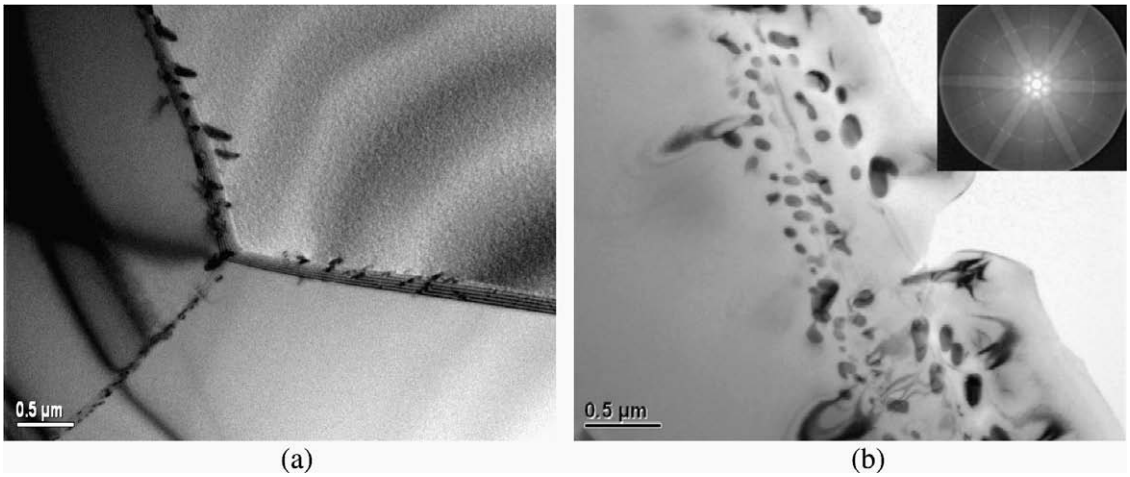

Fig. 7. Representative TEM micrographs showing grain boundary precipitates in the specimens exposed to lithium at 800 °C for (a) 250 h and (b) 500 h.

area electron diffraction patterns. These precipitates were consistent with the fcc plate-shaped Ti(CON) phase which has been reported in V–4Cr–4Ti [16,24,25]. In addition, the plate precipitates also had an orientation relationship with the matrix that was identified as $[001]_{bcc}//[110]_{fcc}$ and $(200)_{bcc}//(200)_{fcc}$, which is the Baker-Nutting orientation relationship [16].

Representative TEM micrographs showing the microstructure for the specimens exposed to lithium at 800 °C for 250 and 500 h are shown in Fig. 7. After 250 h exposure, a few grain boundaries were decorated with a low number density of rod-shaped precipitates, and grain interior was free of precipitates. Further exposure to 500 h significantly increased the number density of grain boundary precipitates, and grain boundaries were heavily decorated by precipitates at both sides of the boundaries, while the grain interior was still free of precipitate particles. The analysis of grain boundary precipitates using convergent beam electron dif-

fraction (CBED) and selected area electron diffraction (SAED) indicated that they were consistent with the fcc Ti(CON) phase. This phase is isomorphous between γ-TiO, TiN, and TiC, which means that the relative interstitial C, O, and N content can vary without changing the crystal structure.

3.5. Changes in electrical resistivity after lithium thermal exposure

The electrical resistivity of V–4Cr–4Ti is sensitive to the content and distribution of interstitial O, N, and C in solid solution and can therefore be used to evaluate the redistribution of interstitial atoms in the solution during exposure treatments. Fig. 8 shows the changes in room-temperature electrical resistivity after each annealing treatment in liquid lithium at 700 and 800 °C. The data points are the averages of the measurements made on individual specimens and the error bars indicate the variation between specimens. The results show that electrical resistivity of V–4Cr–4Ti decreased as exposure time increased at both annealing temperatures. The magnitude of decrease in electrical resistivity at 700 °C (~4 nΩ-m drop after 1000 h exposure) is smaller than that at 800 °C (~10 nΩ-m drop after 1000 h annealing). The decreases in electrical resistivity imply that interstitial solute atoms were removed from solution to form precipitates during lithium exposure.

4. Discussion

Chemical analysis showed significant pickup of nitrogen and retention of oxygen during thermal exposure in lithium at 700 and 800 °C. The level of oxygen dropped only 10 wppm after 1000 h exposure at 700 °C, and 40 wppm after 1000 h exposure at 800 °C. This is in contrast to the depletion of oxygen in V–4Cr–4Ti reported by Grossbeck et al. [26] where ~600 wppm decrease in oxygen concentration was observed after 2500 h exposure in lithium at 800 °C when only slight pickup of nitrogen occurred (~50 wppm N increase for 2500 h). Pickup of nitrogen and retention of oxygen was confirmed in the high-purity NIFS-HEAT-2 tested in the same experiment [5], though the amount of nitrogen and carbon pickup in NIFS-HEAT-2 reported by Nagasaka et al. [5] was much higher than that in US Heat 832665 examined here. The variation was caused primarily by the difference in thickness and overall surface area of coupon specimens. The chemical analysis results therefore, should only be taken as a trend of change in interstitial chemistry.

The oxygen retention in vanadium alloys exposed to lithium was observed in previous studies on V–3Ti–15Nb and V–5Ti–2Cr alloys by Borgstedt et al. [27,28]. There was almost no change in oxygen level and a more than doubled increase in carbon concentration in V–3Ti–15Nb and V–5Ti–2Cr after exposure to lithium at 700 °C for 500 h. Unalloyed vanadium that was tested in the same environment, however, showed a loss of oxygen and a pickup of carbon. It is suggested that the kinetics of interstitial C, N, and O transfer are controlled by both alloying elements and the purity of lithium. When the purity of lithium is maintained, the removal of oxygen is expected in both pure vanadium and vanadium alloys, as predicted by thermodynamics [4]; in low purity lithium, depletion of oxygen in vanadium and retention of oxygen in vanadium alloys occur along with pickup of nitrogen and carbon.

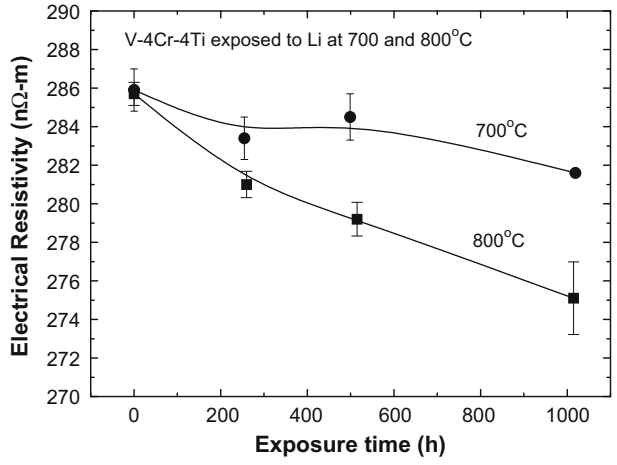

Fig. 8. Changes in room-temperature electrical resistivity of V–4Cr–4Ti after exposures to lithium at 700 and 800 °C.

In spite of significant pickup of nitrogen in V–4Cr–4Ti from the lithium, the matrix concentration of free interstitial solutes was significantly reduced during lithium exposure at both 700 and 800 °C, and this effect was stronger at 800 °C than at 700 °C. This was manifested by a gradual removal of the yield drop and the Lüders strain in the room-temperature stress–strain curves and suppressed serrations in the stress–strain curves at 500 °C. The decrease in room-temperature electrical resistivity of the lithium-exposed specimens also indicated the removal of interstitial solutes from the matrix. According to Matthiessen's rule [29], the resistivity of V–4Cr–4Ti would be increased with increasing contents of interstitial impurities following the relation of:

$$\Delta\rho = \rho_O \Delta x_O + \rho_C \Delta x_C + \rho_N \Delta x_N, \quad (1)$$

where ρ_i and Δx_i are the specific resistivity (nΩ-m/at.%) and the change in atomic concentration of the ith solute species, respectively. The calculated increase in resistivity using the specific resistivity values in the literature and the increase in atomic concentration of O, C, and N from chemical analysis of coupon specimens would be 7–8 nΩ m after 1000 h exposure at 700 and 800 °C. The measured decrease rather than increase in electrical resistivity suggests that a pronounced precipitation process may be occurring in V–4Cr–4Ti during lithium thermal exposure [30].

Enhanced precipitation was observed in V–4Cr–4Ti following lithium exposure. TEM examination of the 700 °C-exposed specimens showed increased precipitation in the matrix and at grain boundaries with increasing exposure time. Strong grain boundary precipitation was observed in the 800 °C-exposed specimens while no precipitation occurred in the grain interior. It is apparent that the precipitates formed in V–4Cr–4Ti during lithium thermal exposure removed not only additional nitrogen solute absorbed from the lithium, but also the interstitial solutes in the original material. Several studies have suggested that almost all nitrogen in V–4Cr–4Ti is contained in titanium precipitates, while oxygen is partitioned between solid solution and precipitates [5,14]. It is uncertain whether or not the kinetics of the oxygen partitioning process was affected by enhanced precipitation reactions associated with nitrogen pickup.

The exposure temperature plays a significant role in the precipitation process in V–4Cr–4Ti. Lithium thermal exposure at 700 °C produced plate-shaped precipitates in the matrix and globular precipitates at the grain boundary, while heterogeneous precipitation at grain boundaries was dominant for lithium exposure at 800 °C. Plate-shaped precipitates in V–4Cr–4Ti have been observed in a variety of experiments below 1000 °C, e.g. neutron irradiation at 510 °C/4 dpa [16] and at 505 °C/0.1 dpa [25], ion irradiation at 600–700 °C/0.75 dpa [31], ion irradiation at 700 °C/3 dpa [19], secondary annealing at 800–900 °C/1 h [15], and post-weld heat treatment at 950 °C/2 h [24], etc. The formation temperature of plate-shaped precipitates varies in the unirradiated and irradiated conditions: >600 °C under thermal annealing and >300 °C under neutron irradiation [9]. The observation of matrix plate-shaped precipitates in the 700 °C-Li-exposed specimens agrees with previous work. The effect of nitrogen pickup on the formation of matrix and grain

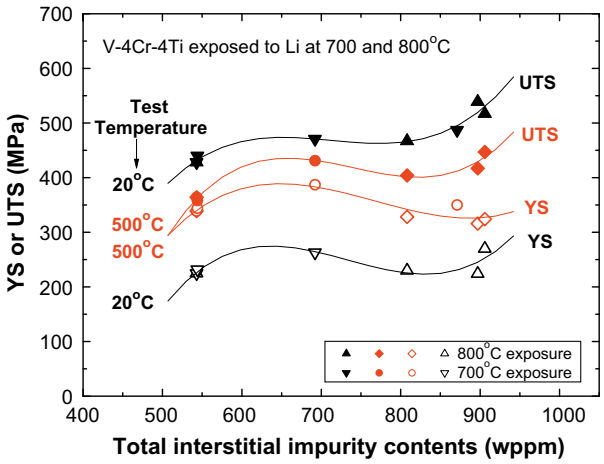

Fig. 9. The yield stress (YS) and the ultimate tensile strength (UTS) vs. total interstitial impurity content in V–4Cr–4Ti tensile tested at 20 and 500 °C.

boundary precipitates can not be differentiated from the effect of thermal treatments in the current lithium experiments. Long-term annealing experiments at 700 °C in a well-controlled vacuum environment is needed to elucidate the influence of interstitial mass transfer in a lithium environment on the precipitation behavior of V–4Cr–4Ti. The extensive precipitation at grain boundaries observed in the 800 °C-Li-exposed specimens has not been reported in previous studies. This preferential grain boundary precipitation was thought to be related to faster diffusion of interstitial atoms along grain boundaries, high mobility of Ti solutes and thermal instability of plate-shaped Ti(CON) phase at 800 °C [5,25]. The dissolution of plate-shaped Ti(CON) precipitates releases Ti into the solution, and Ti solute atoms may diffuse towards grain boundaries as a result of a high concentration of interstitials along grain boundaries, promoting precipitation of globular Ti(CON) particles at grain boundary. It is apparent that globular precipitates are more stable than plate-shaped precipitates at high temperatures, which is consistent with previous findings [16–18]. As the Ti(CON) phase is isomorphous between γ-TiO, TiN, and TiC, it is likely that Ti(CON) precipitates at grain boundaries have a relatively higher N content than Ti(CON) precipitates formed in the matrix.

Though it is impossible to differentiate the roles of individual interstitial elements in determining mechanical performance of V–4Cr–4Ti exposed to liquid lithium, it is believed that the increase in strength and the decrease in ductility in V–4Cr–4Ti following lithium exposure is primarily attributed to nitrogen pickup. Fig. 9 shows the changes in the yield stress and the ultimate tensile strength as a function of the total interstitial impurity concentration in specimens exposed to 700 and 800 °C and tested at 20 and 500 °C. The general trend is that the yield stress and the UTS are sensitive to overall interstitial impurity contents below ~600 ppm and above ~900 ppm, while the tensile stresses are less sensitive to impurity contents between ~600 and 900 ppm. The first hardening regime (below ~600 ppm) is likely associated with solid solution hardening, and the second hardening regime (above ~900 ppm) is perhaps due to precipitation hardening in the grain interior and/or at grain boundaries. Embrittlement is not a concern for V–4Cr–4Ti when the total interstitial impurity concentration is below ~1000 ppm.

5. Conclusions

Lithium exposure led to an increase in strength, a decrease in ductility and a reduced dynamic strain aging effect in V–4Cr–4Ti when the total interstitial impurity concentration increased. No embrittlement was observed, and ductility of V–4Cr–4Ti remained high after 1000 h exposures. Depletion of oxygen did not occur in V–4Cr–4Ti when there was a significant pickup of nitrogen during lithium exposures at 700 and 800 °C. Evident matrix interstitial solute scavenging by precipitation was observed in V–4Cr–4Ti, and precipitation was quite different depending on the exposure temperature. Plate-shaped Ti(CON) precipitates were formed in the matrix and globular precipitates formed at grain boundaries during lithium exposure at 700 °C; only grain boundaries globular precipitates were observed at the exposure temperature of 800 °C.

Acknowledgements

The research was supported by the Office of Fusion Energy Sciences, the US Department of Energy under contract DE-AC05-00OR22725 with Oak Ridge National Laboratory, managed and operated by UT-Battelle, LLC. We would like to thank L.T. Gibson and Janie Myers for their technical support, and Dr S.J. Zinkle for his valuable guidance.

References

[1] T. Muroga, T. Nagasaka, K. Abe, V.M. Chernov, H. Matsui, D.L. Smith, Z.Y. Xu, S.J. Zinkle, J. Nucl. Mater. 307–311 (2002) 547.
[2] R.J. Kurtz, K. Abe, V.M. Chernov, V.A. Kazakov, G.E. Lucas, H. Matsui, T. Muroga, G.R. Odette, D.L. Smith, S.J. Zinkle, J. Nucl. Mater. 283–287 (2000) 70.
[3] D.R. Diercks, B.A. Loomis, J. Nucl. Mater. 141–143 (1986) 1117.
[4] D.L. Smith, K. Natesan, Nucl. Technol. 22 (1974) 392.
[5] T. Nagasaka, T. Muroga, M. Li, D.T. Hoelzer, S.J. Zinkle, M.L. Grossbeck, H. Matsui, Fus. Eng. Des. 81 (2006) 307.
[6] Meimei Li, T. Nagasaka, D.T. Hoelzer, M.L. Grossbeck, S.J. Zinkle, T. Muroga, K. Fukumoto, H. Matsui, M. Narui, J. Nucl. Mater. 367–370 (2007) 984.
[7] T. Nagasaka, H. Takahashi, T. Muroga, T. Tanabe, H. Matsui, J. Nucl. Mater. 283–287 (2000) 816.
[8] M. Satou, T. Chuto, K. Abe, J. Nucl. Mater. 283–287 (2000) 367.
[9] R.J. Kurtz, K. Abe, V.M. Chernov, D.T. Hoelzer, H. Matsui, T. Muroga, G.R. Odette, J. Nucl. Mater. 329–333 (2004) 47.
[10] S.J. Zinkle, H. Matsui, D.L. Smith, A.F. Rowcliffe, E. van Osch, K. Abe, V.A. Kazakov, J. Nucl. Mater. 258–263 (1998) 205.
[11] M. Koyama, K. Fukumoto, H. Matsui, J. Nucl. Mater. 329–333 (2004) 442.
[12] D.L. Smith, R. Lee, R. Yonco, in: Proceedings of Second International Conference on Liquid Metal Technology in Energy Production, Richland, WA, USA, 1980, p. 2.
[13] M. Satou, H.M. Chung, Fusion Reactor Materials Semiannual Progress Report, DOE/ER-0313/13, 1992, p. 227.
[14] N.J. Neo, T. Nagasaka, T. Muroga, H. Matsui, J. Nucl. Mater. 307–311 (2002) 620.
[15] A. Nishimura, A. Iwahori, N.J. Neo, T. Nagasaka, T. Muroga, S.I. Tanaka, J. Nucl. Mater. 329–333 (2004) 438.
[16] D.T. Hoelzer, S.J. Zinkle, Fusion Materials Semiannual Progress Report, DOE/ER-0313/29, 2000, p. 19.
[17] D.T. Hoelzer, A.F. Rowcliffe, M. Li, Fusion Materials Semiannual Progress Report, DOE/ER-0313/38, 2005, p. 2.
[18] D.T. Hoelzer, Fusion Materials Semiannual Progress Report, DOE/ER-0313/25, 1998, p. 59.
[19] M. Hatakeyama, H. Watanabe, T. Muroga, N. Yoshida, J. Nucl. Mater. 329–333 (2004) 420.
[20] D.T. Hoelzer, A.F. Rowcliffe, J. Nucl. Mater. 307–311 (2002) 596.
[21] M.L. Grossbeck, J. Nucl. Mater. 307–311 (2002) 615.
[22] M.L. Grossbeck, Fusion Materials Semiannual Progress Report, DOE/ER-0313/30, 2001, p. 8.
[23] D.L. Harrod, R.E. Gold, Int. Metals Rev. 4 (1980) 163.
[24] M.L. Grossbeck, J.F. King, D.J. Alexander, P.M. Rice, G.M. Goodwin, J. Nucl. Mater. 258–263 (1998) 1369.
[25] P.M. Rice, S.J. Zinkle, J. Nucl. Mater. 258–263 (1998) 1414.
[26] M.L. Grossbeck, L.T. Gibson, M.J. Gardner, Fusion Materials Semiannual Progress Report, DOE/ER-0313/32, 2002, p. 6.
[27] H.U. Borgstedt, J. Nucl. Mater. 51 (1974) 221.
[28] H.U. Borgstedt, Wekstoffe und Korrosion 28 (1977) 529.
[29] G.T. Meadon, Electrical Resistance of Metals, New York, Plenum, 1965.
[30] S.J. Zinkle, A.N. Gubbi, W.S. Eatherly, Fusion Materials Semiannual Progress Report, DOE/ER-0313/21, 1996, p. 15.
[31] H. Watanabe, M. Suda, T. Muroga, N. Yoshida, J. Nucl. Mater. 307–311 (2002) 408.